

# Optical field-enhancement and sub-wavelength field-confinement using excitonic nanostructures

M. J. Gentile,<sup>\*,†</sup> S. Núñez-Sánchez,<sup>\*,†</sup> and W. L. Barnes<sup>\*,†,‡</sup>

*School of Physics and Astronomy, University of Exeter, Exeter EX4 4QL, U.K., and Complex Photonic Systems (COPS), MESA+ Institute for Nanotechnology, University of Twente, 7500 AE Enschede, The Netherlands*

E-mail: m.j.gentile@exeter.ac.uk; sara.nunez.sanchez@gmail.com; W.L.Barnes@exeter.ac.uk

## Abstract

We show that dye-doped polymers open an interesting route to controlling light at the nanoscale. Just as for the much better known metal-based plasmonic systems, propagating and localized modes are possible. We show that the attractive features offered by plasmonics, specifically enhanced optical fields and sub-wavelength field confinement, are also available with these materials. They thus open a new opportunity in nanophotonics in which fabrication and functionality might be achieved by harnessing molecular and supramolecular chemistry.

Much is expected of plasmonics, with applications being pursued over a wide range of fields from on-chip plasmonic circuits<sup>1</sup> to nanoantennae for the emission of light.<sup>2</sup> The key to this wide-ranging interest is that plasmonics enables the control of light deep into the sub-wavelength regime, right down to the nanoscale.<sup>3</sup> Noble metals such as gold and silver have fuelled the plasmonics

---

\*To whom correspondence should be addressed

<sup>†</sup>School of Physics and Astronomy, University of Exeter, Exeter EX4 4QL, U.K.

<sup>‡</sup>Complex Photonic Systems (COPS), MESA+ Institute for Nanotechnology, University of Twente, 7500 AE Enschede, The Netherlands

revolution, providing a strong plasmonic response in the visible part of the electromagnetic spectrum. Their plasmonic response is associated with a negative real part of their permittivity,  $\epsilon'$ , in this frequency range. For several decades it has been appreciated that loss (absorption) associated with metals places a limitation on, for example, the distance over which surface plasmon-polariton modes (SPPs) may propagate and these losses are associated with the imaginary part of the permittivity,  $\epsilon''$ . Many have sought to find ways to reduce these losses, for example by adding gain materials to plasmonic nanostructures so as to offset the losses,<sup>4</sup> or by seeking alternative materials to the noble metals.

A variety of alternative materials have been explored, including: doped semiconductors,<sup>5</sup> graphene,<sup>6</sup> chalcogenides,<sup>7</sup> tunable metal-semiconductor materials,<sup>8,9</sup> transparent conducting oxides,<sup>10</sup> heavily-doped conducting polymers,<sup>11</sup> and some nitrides,<sup>12,13</sup> among others. All of these materials yield a plasmonic response owing to the free charge-carriers they contain. The simplest model for the permittivity of a material whose electromagnetic response is dominated by free carriers is the Drude model, for which the permittivity is given by,<sup>14</sup>

$$\epsilon(\omega) = 1 - \frac{\omega_p^2}{\omega^2 - i\omega\gamma} \quad (1)$$

where  $\omega_p$  is the plasma frequency and  $\gamma$  is the damping rate. This Drude response yields a negative permittivity provided  $\omega < \omega_p$ . The types of plasmon modes that may be supported depend on how negative the permittivity is: propagating SPP modes require  $\epsilon'(\omega) \leq -1$  whilst localised SPP modes require  $\epsilon'(\omega) \leq -2$ .<sup>14</sup>

In plasmonic materials the negative permittivity is a consequence of the way the free charge-carriers (typically a plasma of conduction electrons) respond to an applied electromagnetic field. However, this is not the only way a negative permittivity may arise: it may also occur in the (spectral) vicinity of a strong absorption resonance. In the work presented here our interest lies in resonances associated with a strong yet narrow absorption line, typically due to exciton excitation. The relative permittivity of a material that involves several resonances ( $i = 0, 1, 2..$ ) may be accounted for using the Lorentz model,<sup>15,16</sup>

$$\varepsilon(\omega) = \varepsilon_b + \sum_i \frac{f_i \omega_i^2}{\omega_i^2 - \omega^2 - i\omega\gamma_i}. \quad (2)$$

In many cases one resonance dominates so that  $\omega_0$  is the frequency associated with the transition (the resonant frequency),  $f_0$  is the reduced oscillator strength<sup>17</sup> of the transition and  $\gamma_0$  is the damping rate. The term  $\varepsilon_b$  takes account of any non-resonant (background) response that may be associated with other transitions well away (spectrally) from the transition of interest. The properties of a material for which the Lorentz model is appropriate depend strongly on  $f_0$ : if  $f_0$  is sufficiently large then the real part of the permittivity will become negative and the material will take on a metal-like appearance over a small wavelength range below the exciton resonance.<sup>18</sup>

In appropriate frequency ranges plasmonic and excitonic materials may both exhibit negative permittivities, but they do so for very different reasons. The negative permittivity of plasmonic materials arises from the mobile conduction electrons whilst the negative permittivity of excitonic materials considered here arises from the nature of the localized Frenkel electron-hole pairs they support. Our purpose here is to show, through experiment and simulation, that plasmonic materials are not the only way to achieve optical field enhancement and sub-wavelength field confinement; nanostructured excitonic materials may be used for the same purpose.

Just as plasmonic materials can support SPP modes so too can excitonic materials, in which case we refer to them as surface exciton-polaritons (SEPs).<sup>19</sup> Surface polaritons based on excitonic materials have been known for many years. Early work involved materials that needed low temperatures, both inorganic solids: ZnO,<sup>19</sup> CuBr,<sup>20</sup> ZnSe,<sup>21</sup> CuCl,<sup>22</sup> and one organic solid, anthracene.<sup>23</sup> Some organic dye molecules also exhibit strong, narrow excitonic absorption bands, for example J-aggregated dye molecules.<sup>24–26</sup> Swalen and co-workers made important contributions in the late 1970s and early 1980s by showing that surface polaritons based on the excitonic response of a variety of dye molecules could be achieved at room temperature.<sup>27–32</sup> More recently this work has been picked up by Gu *et al.*<sup>33</sup> (Gu *et al.* referred to their mode by using the appealing phrase 'organic plasmon', this seems inappropriate: whilst the system is made of organic molecules, the response is due to excitons associated with the dye molecules, not a plasma associ-

ated with free charge carriers).

Previous work has demonstrated that propagating SEP modes are possible using dye-molecule based excitonic materials; here we show that localised SEP modes are also possible. Furthermore, we show that localised SEPs have the potential to help us manipulate light at the nanoscale in much the same way as localised SPPs. The rapid expansion of the field of plasmonics owes its origins to improved nano-fabrication techniques, new nano-optical characterisation tools and better modelling capabilities: excitonic materials may now perhaps benefit in the same way. We chose to work with dye-doped polymers in this study for two reasons: first, this allowed us to adjust the doping level and therefore control the effective oscillator strength,  $f_0$ . Second, such an approach lends itself to interesting design and fabrication routes, rational design for the dyes can be accomplished through chemical synthesis,<sup>34,35</sup> whilst nanostructuring of polymers may be achieved by, for example, conformal imprint lithography,<sup>36</sup> or self assembly.<sup>37</sup> There is the prospect of all optical functionality.<sup>38</sup>

Below we present our results for polyvinyl alcohol (PVA) thin films doped with J-aggregated molecules (TDBC: 5,6-dichloro-2-[[5,6-dichloro-1-ethyl-3-(4-sulphobutyl)-benzimidazol-2-ylidene]-propenyl]-1-ethyl-3-(4-sulphobutyl)-benzimidazolium hydroxide, sodium salt, inner salt) used as obtained from Few Chemicals GmbH. The TDBC doped PVA (TDBC:PVA) thin films were prepared on glass substrates by spin coating from water-based solutions. The dye-polymer solutions were prepared by mixing a 6.0 wt% PVA-water solution with a 2.0 wt% TDBC-water solution of in a 1:3 volume ratio. The initial PVA (molar weight 85 000-124 000) solution was prepared by dissolving the PVA in hot water at 90° C for several hours, yielding a 6.0 wt% solution that was cooled before mixing with the TDBC-water solution. The final TDBC-PVA water solution had a composition of 1.5 wt% PVA and 1.46 wt% TDBC. After deposition by spin coating the thickness of the resulting films were characterized using a surface profiler (KLA D-100).

The metal-like optical properties of this type of sample are shown in the photograph in Figure 1, where the TDBC:PVA film shows a similar colour in reflected light to a gold film. This similarity is related to the metal-like optical properties that the dye-doped polymer exhibits in the

yellow/orange spectral region, below the exciton resonance at  $590\text{nm}$ . Specifically, the metallic copper-like reflectance of the TDBC:PVA film arises because of the strong (negative) real permittivity in the orange part of the spectrum whilst the autumn yellow colour is due to inter-band absorption towards the blue end of the spectrum.<sup>39</sup> The key point is that TDBC-doped PVA has a sufficiently strong permittivity to give a metal-like appearance.

To determine the permittivity of our films we measured their reflectance and transmittance at normal incidence as a function of wavelength. We then used a parameter retrieval process to extract the frequency dependent permittivity. This procedure was based on fitting numerically-simulated data based on Fresnel equations<sup>40</sup> to the experimental data, a Kramers-Krönig (KK) analysis being used to help select the most physically appropriate solution (see Supporting Information). The results of such a process for a  $70 \pm 7\text{ nm}$ -thick J-aggregated film spun from a TDBC-PVA water solution containing 1.46 wt% TDBC are shown in Figure 2.

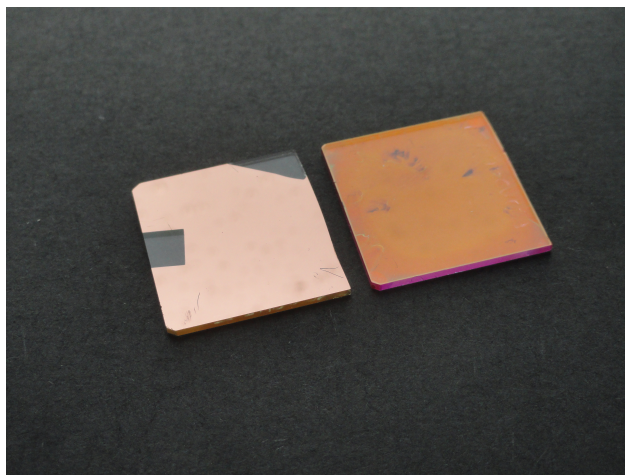


Figure 1: Photograph of a dye film spun from a TDBC-PVA water solution containing 1.46 wt% TDBC (top right) along with a gold film for comparison (lower left).

Also shown in Figure 2 are the results of fitting a two-oscillator Lorentz model to the extracted data.

To show that our TDBC:PVA films are capable of supporting SPEs we followed Philpott *et al.*<sup>29</sup> and Gu *et al.*<sup>33</sup> and used the attenuated total reflection technique in the Kretschmann-Raether prism coupling geometry<sup>41</sup> to measure the reflectivity of thin TDBC:PVA films; the resulting data

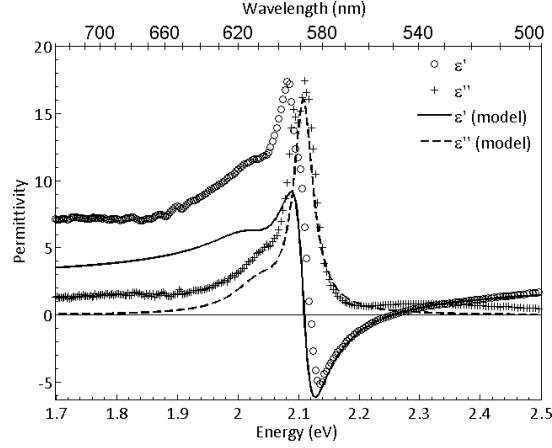


Figure 2: Extracted values of the real (circles) and imaginary (crosses) parts of the permittivity of a thin film spun from a TDBC-PVA water solution containing 1.46 wt% TDBC. Also shown are the results of fitting a two-oscillator Lorentz model to these data (lines). The best-fit parameters were determined to be  $\omega_0 = 2.10\text{eV}$  (590nm),  $\gamma_0 = 0.053\text{eV}$ ,  $\epsilon_b = 2.310$ ,  $f_0 = 0.36$ ,  $\omega_1 = 2.03\text{eV}$  (610nm),  $\gamma_1 = 0.0988\text{eV}$  and  $f_1 = 0.10$  (for details of the parameter extraction see the supporting information).

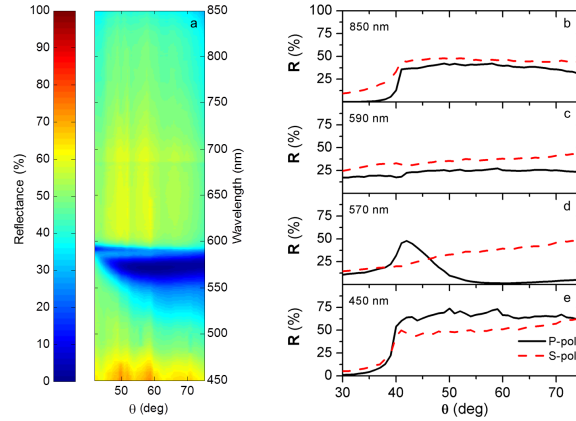


Figure 3: Left: reflectance of a nominally 70 nm thick film spun from a TDBC-PVA water solution containing 1.46 wt% TDBC: (a) P-polarised reflectance ( $R_P$ ) colour map as a function of wavelength and incident angle. Right: reflectance for both P- and S-polarisations for incident wavelengths of: (b) 850 nm, (c) 590 nm, (d) 570 nm and (e) 450 nm.

are shown in Figure 3. We used a white light source followed by a scanning monochromator for our incident beam, thereby allowing a spectral range from 1.46 eV (850 nm) to 2.76 eV (450 nm) to be swept. Panel (a) in Figure 3 shows the p-polarised reflectance,  $R_P$ , obtained for a nominally 70 nm thick film spun from a TDBC-PVA water solution (containing 1.46 wt% TDBC) as a function of

the wavelength and the incident angle. The  $R_P$  response shows a dip as a function of incident angle for wavelengths between 530 and 585 nm, below the exciton absorption resonance at 590 nm. For wavelengths far removed from the exciton absorption  $R_P$  is (as expected) rather featureless. This is also evident in Figure 3b and Figure 3e where single wavelength reflectance data are shown for  $R_P$  and  $R_S$  at wavelengths of 850 nm and 450 nm respectively. The only feature that these data show is the critical angle at  $\sim 41^\circ$ . At the exciton transition peak, 590 nm,  $R_P$  and  $R_S$  are both dominated by absorption, the reflectance for both polarisations being low and largely angle-independent (Figure 3c). By contrast, at a wavelength of 570 nm,  $R_P$  shows a gradual decrease for angles beyond the critical angle until it reaches a minimum near  $62^\circ$ . For angles larger than the critical angle  $R_S$  shows a monotonically rising response (Figure 3d).

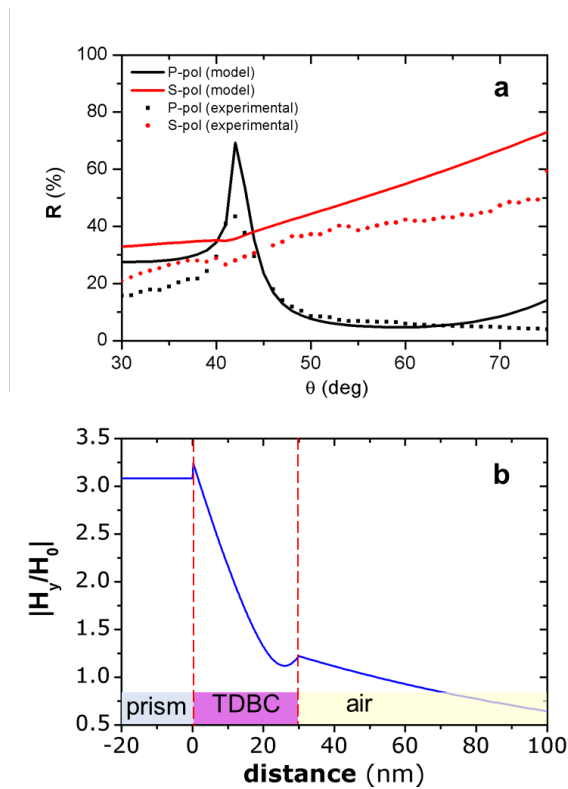


Figure 4: Upper (a)  $R_P$  and  $R_S$  experimental (dotted lines) and model data (solid lines) for a thin film spun from a TDBC:PVA solution containing 1.46 wt% TDBC at a wavelength of 579 nm. The model parameters used here were: film thickness 30 nm, permittivity of spun film  $-4.4 + 9.9i$ , permittivity of prism 2.28. Lower (b) calculated magnitude of the local magnetic field strength ( $H_y$  component) for p-polarised incident light, at a wavelength of 579 nm, and for an angle of incidence of  $60^\circ$  as a function of distance through the structure.

To explore the nature of the broad minimum in the p-polarised reflectance ( $R_P$ ) seen in Figure 3d, we fitted modelled reflectance data to the experimentally acquired data using a recursive Fresnel approach. Figure 4a shows the  $R_P$  and  $R_S$  experimental (dotted lines) and modelled (solid lines) data for a wavelength of 579 nm. The fitted value of the permittivity for this TDBC:PVA thin film was  $-4.4 + 9.9i$ . This compares with the value used at the start of the fitting process (taken from the parameter retrieval process, see Figure 2) of  $-4.4 + 3.9i$ . The higher value of the imaginary part of the fitted permittivity is probably due to the presence of surface roughness of the spun film, the roughness leads to losses that in a simple approximation can be incorporated into  $\epsilon''$ .<sup>42</sup> Losses due to surface roughness are likely to be more apparent when a surface mode is excited (as here) than for normal incidence illumination (as for our parameter retrieval procedure). We have also calculated<sup>43</sup> and plotted the magnetic component of the p-polarised optical field through the sample for the same incident wavelength and angle in Figure 4b. In this figure two features are apparent: first, going from the prism/TDBC:PVA interface into the TDBC:PVA film the field decays with distance - this is expected for an absorbing film; second, the field rises again towards the TDBC:PVA/air interface - indeed, the field decays on either side of the TDBC:PVA interface, just as expected for a surface mode.<sup>29</sup> These data (Figure 4) allow us to identify the reflectivity minimum with the excitation of a SEP mode.

Having established that our TDBC:PVA films may support a propagating surface exciton-polariton we now turn our attention to localised (particle) surface exciton-polariton modes. The data presented in Figure 2 indicate that over a small spectral range the real part of the permittivity of our film goes below -2; this material should therefore be able to support localised modes. We used Mie theory<sup>44</sup> to calculate the absorption efficiency of 100 nm-diameter nanospheres using a single-oscillator Lorentz model (for a range of oscillator strengths) and employed the extracted values of the permittivity presented in Figure 2; the resulting data are shown in Figure 5a. We chose a single-oscillator model so as to make the evolution of the response with oscillator strength clear. The bare exciton absorption position is shown as a vertical dotted line. These data show a transition in the behaviour of the absorption efficiency as the oscillator strength is increased. The

absorption efficiency is defined as the absorption cross-section divided by the geometrical cross-section (note that the data for different oscillator strengths are offset vertically for clarity). For low oscillator strengths, *e.g.*  $f_0 = 0.05$  (dotted line), the only feature present is the exciton absorption at  $2.10 \text{ eV}$  ( $590 \text{ nm}$ ), very close to the bare exciton frequency. For stronger oscillator strengths, *e.g.*  $f_0 = 0.36$  (solid line), the peak in the absorption efficiency moves to higher frequencies (shorter wavelengths)  $\sim 2.18 \text{ eV}$ . This shift occurs because for these higher oscillator strengths the real part of the permittivity extends below  $-2$  so that localised surface modes may be supported; the  $\sim 2.18 \text{ eV}$  peak in the absorption efficiency corresponds to this condition. The absorption efficiency spectrum calculated using the extracted (experimental) permittivity values (dash-dotted line) looks very similar.

For the propagating SEP mode discussed above we confirmed the surface nature of the mode from the calculated field profile in Figure 4b; we can now do something similar for the localised mode. In Figure 5b we plot the time and surface averaged electric field strength (normalised to the incident field strength) for a  $100 \text{ nm}$  diameter sphere of our TDBC:PVA (crosses and dots, indicating data based on permittivity values derived from parameter retrieval and fitted reflectivity respectively) and a  $132 \text{ nm}$  diameter gold sphere for comparison (dashed line). These data were again calculated using Mie theory. The diameter of the gold sphere was chosen so as to give a resonance at the same frequency as the TDBC:PVA sphere. The results of two calculations are shown, one using permittivity values obtained from the parameter retrieval process (see Figure 2), referred to in Figure 5b as ‘smooth’ and indicated by crosses, the other using permittivity values obtained from fitting modeled reflectivity data, Figure 3 Figure 4, and referred to in the figure as ‘rough’ and indicated by dots (‘rough’ refers to the fact that the difference in these permittivity values when compared to those derived from the parameter retrieval process arise from the way the roughness of the doped PVA films affects the reflectivity measurements). Importantly, for both parameter sets, there is a clear enhancement of the surface electric field on resonance. For the lower loss permittivity values (smooth, crosses) the enhancement is greater than that of a comparable gold particle on resonance (dashed line). Two further differences may be observed: first, the field

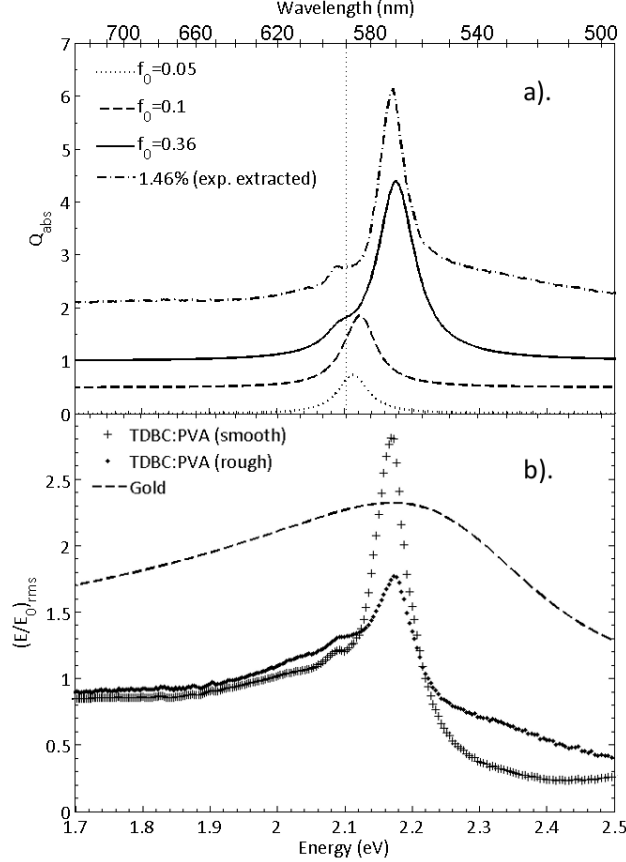


Figure 5: Upper (a). The absorption efficiency ( $Q_{abs}$ ) for 100 nm-diameter nanospheres of TDBC:PVA using a single-oscillator Lorentz model for three different effective oscillator strengths (concentrations) together with the absorption efficiency calculated using the experimentally-extracted permittivity (dash-dotted line). The exciton transition energy in the Lorentz model is marked with the vertical dotted line. Lower (b). The time-averaged (root mean square) of the calculated average electric field strength over the surface of a 100 nm diameter particle of TDBC:PVA. The results of a similar calculation for a spherical gold particle are also shown (dashed line) gold. The diameter of the gold sphere 132 nm was chosen to provide a resonance that peaks at the same spectral position as that of the 100 nm TDBC:PVA particle. The shoulder near 2.1 eV in the TDBC:PVA data corresponds to the bare exciton absorption. For the distinction between ‘rough’ and ‘smooth’ see main text

enhancement for the excitonic system is spectrally much sharper than that of the gold particle. This sharp response is a natural consequence of the narrow spectral range over which the permittivity of the TDBC:PVA is sufficiently negative. Second (and perhaps rather surprisingly) the maximum field enhancement for the TDBC:PVA particle (lower loss parameters) is greater than that of the gold particle. At the resonant frequency the permittivity of the gold takes the values  $-7.20 + 1.70i$  whilst that of the TDBC:PVA (from parameter retrieval) is  $-2.55 + 1.24i$ .

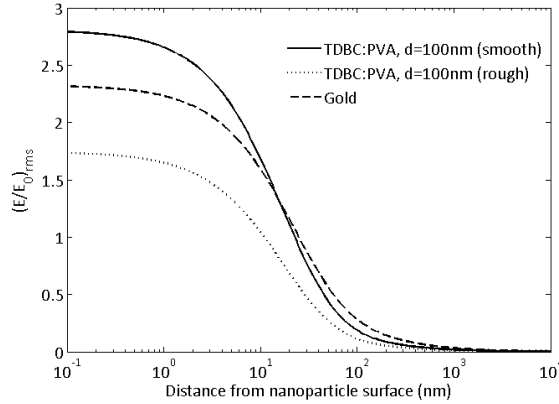


Figure 6: The strength of the time-averaged and orientationally-averaged electric field strength as a function of distance from the surface of the sphere for the TDBC:PVA sphere (solid line) and a gold sphere (dashed line).

Field enhancement on resonance such as that shown in Figure 5b is a key signature of localised modes; so too is the confinement of the field. In Figure 6 we show the calculated spatial field distribution associated with TDBC:PVA and gold particles explored in Figure 5b. Again, these data were calculated using Mie theory. Again the results of two calculations are shown, one using permittivity values obtained from the parameter retrieval process, ‘smooth’ and indicated by the solid line, the other using permittivity values obtained from fitting modeled reflectivity data, ‘rough’ and indicated by the dotted line. For both parameter sets we see that the field associated with the localized surface exciton-polariton mode is tightly confined to the vicinity of the particle just as the field associated with the localized surface plasmon-polariton mode of the gold particle is, both decaying with a characteristic distance of  $\sim 20 \text{ nm}$ .

In summary, we have shown that polymer films doped with J-aggregated (TDBC) molecules may exhibit a negative real permittivity in the vicinity of the exciton resonance. We have shown that thin films of such material may support surface exciton-polariton modes, in much the same way that thin metal films support surface plasmon-polariton modes. Furthermore, we have used the material parameters derived from experiment to demonstrate that nano-structured excitonic materials may support localised surface exciton-polariton modes. Thus, we have shown that the two key attributes of plasmonics (field enhancement and confinement) may be achieved by exploitation of

exciton-polaritons. With this in mind we suggest that these excitonic materials offer an interesting and alternative path to controlling light at the nanoscale. This approach also offers the prospect of being able to tailor material properties through the design of appropriate excitonic (dye) molecules using the powerful techniques of supramolecular chemistry. The use of doped polymers opens up the possibility of nanostructuring via easily scaled-up processes such as conformal imprint lithography. Finally, although the speed of the typical excitonic response ( $\sim 10^{-10}$  s)<sup>45</sup> does not match that for plasmonic systems ( $\sim 10^{-14}$  s),<sup>46</sup> this approach offers the prospect of dynamical optical control of these material properties (and hence nanophotonic functionality) by appropriate pumping of the excitonic transition.

Supporting Information Available: [concerning refractive index retrieval] This material is available free of charge via the Internet at <http://pubs.acs.org>.

## Acknowledgements

SNS gratefully acknowledges the support of the Spanish Government through a Spanish MEC D EX-2010-1009 fellowship (I-D+i 2008-2011 national plan). WLB gratefully acknowledges the support of The Leverhulme Trust and the Royal Society who provided support via an International Exchange Scheme. The authors declare no competing financial interest.

## References

- [1] Ebbesen, T. W.; Genet, C.; Bozhevolnyi, S. I. *Physics Today* **2008**, *61*, 44–50.
- [2] Curto, A. G.; Volpe, G.; Taminiau, T. H.; Kreuzer, M. P.; Quidant, R.; van Hulst, N. F. *Science* **2010**, *329*, 930–933.
- [3] Gramotnev, D.; Bozhevolnyi, S. *Nature Photonics* **2010**, *4*, 83–91.
- [4] Berini, P.; De Leon, I. *Nature Photonics* **2012**, *6*, 16–24.

- [5] Law, S.; Yu, L.; Rosenberg, A.; Wasserman, D. *Nano Letters* **2013**, *13*, 4569–4574.
- [6] Thongrattanasiri, S.; Silveiro, I.; Garcia de Abajo, F. J. *Applied Physics Letters* **2012**, *100*, 201105.
- [7] Maharana, P. K.; Jha, R. *Sensors and Actuators B: Chemical* **2012**, *169*, 161–166.
- [8] Wang, L.; Radue, E.; Kittiwatanakul, S.; Clavero, C.; Lu, J.; Wolf, S. A.; Novikova, I.; Lukaszew, R. A. *Optics Letters* **2012**, *37*, 4335–4337.
- [9] Appavoo, K.; Lei, D. Y.; Sonnefraud, Y.; Wang, B.; Pantelides, S. T.; Maier, S. A.; Haglund, R. F. *Nano Letters* **2012**, *12*, 780–786.
- [10] Rhodes, C.; Franzen, S.; Maria, J.; Losego, M.; Leonard, D.; Laughlin, B.; Duscher, G.; Weibel, S. *Journal of Applied Physics* **2006**, *100*, 054905.
- [11] Matsui, T.; Vardeny, Z. V.; Agrawal, A.; Nahata, A.; Menon, R. *Applied Physics Letters* **2006**, *88*, 071101.
- [12] Naik, G. V.; Liu, J.; Kildishev, A. V.; Shalaev, V. M.; Boltasseva, A. *Proceedings of the National Academy of Sciences* **2012**, *109*, 8834–8838.
- [13] Naik, G. V.; Schroeder, J. L.; Ni, X.; Kildishev, A. V.; Sands, T. D.; Boltasseva, A. *Optical Materials Express* **2012**, *2*, 478–489.
- [14] Le Ru, E. C.; Etchegoin, P. G. *Principles of Surface-Enhanced Raman Spectroscopy and related plasmonic effects*, 1st ed.; Elsevier, 2009.
- [15] Fox, M. *Optical Properties of Solids*, 2nd ed.; Oxford University Press: Oxford, 2010.
- [16] Lebedev, V. S. *Quantum Electronics* **2012**, *42*, 701–713.
- [17] Pockrand, I.; Swalen, J. D.; Gordon II, J. G.; Philpott, M. R. *The Journal of Chemical Physics* **1979**, *70*, 3401–3408.

- [18] Anex, B. G.; Simpson, W. *Reviews of Modern Physics* **1960**, *32*, 466–476.
- [19] Lagois, J.; Fischer, B. *Physical Review Letters* **1976**, *36*, 680–683.
- [20] Hirabayashi, I.; Koda, T.; Tokura, Y.; Murata, J.; Kaneko, Y. *Journal of the Physical Society of Japan* **1976**, *40*, 1215–1216.
- [21] Tokura, Y.; Hirabayashi, I.; Koda, T. *Journal of the Physical Society of Japan* **1977**, *42*, 1071–1072.
- [22] Hirabayashi, I.; Koda, T.; Tokura, Y.; Murata, J.; Kaneko, Y. *Journal of the Physical Society of Japan* **1977**, *43*, 173–180.
- [23] Tomioka, K.; Sceats, M. G.; Rice, S. A. *The Journal of Chemical Physics* **1977**, *66*, 2984–2993.
- [24] Lidzey, D. G.; Bradley, D. D. C.; Virgili, T.; Armitage, A.; Skolnick, M. S. *Physical Review Letters* **1999**, *82*, 3316–3319.
- [25] Bradley, M. S.; Tischler, J. R.; Bulović, V. *Advanced Materials* **2005**, *17*, 1881–1886.
- [26] Dintinger, J.; Klein, S.; Bustos, F.; Barnes, W. L.; Ebbesen, T. W. *Physical Review B* **2005**, *71*, 035424.
- [27] Pockrand, I.; Brillante, A.; Philpott, M.; Swalen, J. *Optics Communications* **1978**, *27*, 91–94.
- [28] Brillante, A.; Pockrand, I.; Philpott, M. R.; Swalen, J. D. *Chemical Physics Letters* **1978**, *57*, 395.
- [29] Philpott, M. R.; Brillante, A.; Pockrand, I.; Swalen, J. D. *Molecular Crystals and Liquid Crystals* **1979**, *50*, 139–162.
- [30] Brillante, A.; Philpott, M. R.; Pockrand, I. *The Journal of Chemical Physics* **1979**, *70*, 5739–5746.

- [31] Philpott, M. R.; Pockrand, I.; Brillante, A.; Swalen, J. D. *The Journal of Chemical Physics* **1980**, *72*, 2774–2787.
- [32] Pockrand, I.; Brillante, A.; Möbius, D. *The Journal of Chemical Physics* **1982**, *77*, 6289.
- [33] Gu, L.; Livenere, J.; Zhu, G.; Narimanov, E. E.; Noginov, M. a. *Applied Physics Letters* **2013**, *103*, 021104.
- [34] Lehn, J.-M. *Supramolecular Chemistry: Concepts and Perspectives*, 1st ed.; Wiley VCH, 1995.
- [35] Feng, J.; Jiao, Y.; Ma, W.; Nazeeruddin, M. D.; Gratzel, M.; Meng, S. *Journal of Physical Chemistry C* **2013**, *117*, 3772.
- [36] Rodriguez, S.; Abass, A.; Maes, B.; Janssen, O.; Vecchi, G.; Gómez Rivas, J. *Physical Review X* **2011**, *1*, 021019.
- [37] van Hameren, R.; Schon, P.; van Buul, A. M.; Hoogboom, J.; Lazarenko, S. V.; Gerritsen, J. W.; Engelkamp, H.; Christianen, P. C. M.; Heus, H. A.; Mann, J. C.; Rasing, T.; Speller, S.; Rowan, A. E.; Elemans, J. A. A. W.; Nolte, R. J. M. *Science* **2006**, *314*, 1433–1436.
- [38] Senge, M. O.; Fazekas, M.; Notaras, E. G. a.; Blau, W. J.; Zawadzka, M.; Locos, O. B.; Ni Mhuircheartaigh, E. M. *Advanced Materials* **2007**, *19*, 2737–2774.
- [39] Pyykko, P.; Desclaux, J. *Accounts of Chemical Research* **1979**, *12*, 276–281.
- [40] Azzam, R. M. A.; Bashara, N. M. *Ellipsometry and polarized light*, 1st ed.; North-Holland, 1977.
- [41] Kretschmann, E.; Raether, H. *Zeitschrift für Naturforschung A* **1968**, *23*, 2135–2136.
- [42] Nash, D. J.; Sambles, J. R. *Journal of Modern Optics* **1999**, *46*, 1793–1800.

- [43] Smith, L. H.; Taylor, M. C.; Hooper, I. R.; Barnes, W. L. *Journal of Modern Optics* **2008**, *55*, 2929–2943.
- [44] Bohren, C. F.; Huffman, D. R. *Absorption and scattering of light by small particles*; Wiley-VCH, 2004.
- [45] Sundstrom, V.; Gillbro, T.; Gadonas, R. A.; Piskarskas, A. *Journal of Physical Chemistry* **1988**, *89*, 2754–2762.
- [46] Sönnichsen, C.; Franzl, T.; Wilk, T.; von Plessen, G.; Feldmann, J. *Physical Review Letters* **2002**, *88*, 077402.

# Graphical TOC Entry

